3D fruit microstructure characterization using micro-CT imaging and deep learning-based panoptic segmentation

Leen Van Doorselaer[1], Dr. Pieter Verboven[1], Prof. Bart Nicolaï[1,2]
[1]BIOSYST-MeBioS, Postharvest group, KU Leuven, Leuven, Belgium, [2]VCBT, Leuven, Belgium

Background
Metabolic processes in plants involving transport of water, metabolic gasses, and nutrients are controlled by the three-dimensional (3D) microscopic morphology of the plant tissues. However, imaging and quantifying this microstructure, including the spatial layout of cells, pores (intercellular spaces) and vascular bundles, is a challenging task.

X-ray micro-computed tomography (micro-CT) has been proposed for 3D plant tissue imaging. This advanced imaging technique requires little preparation and resolves easily pore and cell phases due to differences in attenuation. X-ray micro-CT also covers a large field of view compared to other microscopy techniques, thus rendering more representative volumes of interest.

To quantify plant tissue morphology, the tomographic images require extensive image processing, which can become time-consuming and labor-intensive. Cell segmentation in particular is a difficult task because of low contrast in X-ray attenuation at cell-to-cell interfaces.

Deep learning (DL) is increasingly being used for complex image processing tasks in various fields. DL models can be trained to predict semantic labels where each pixel or voxel is assigned to a class label. Cell segmentation, however, is an instance segmentation task, where pixels or voxels of the same class are assigned to separate instances.

This work aims to speed up and improve 3D plant tissue microstructure characterization using X-ray micro-CT imaging and DL-based models for panoptic segmentation, which combines semantic and instance segmentation tasks. The method was developed and validated for pome fruit tissue samples.

Methods
An X-ray micro-CT dataset was collected to develop panoptic segmentation models. This dataset consisted of pairs of conventional and contrast-enhanced X-ray micro-CT images of the same tissue sample. Pear and apple fruit were sampled at three different radial positions. Different cultivars were compared. X-ray projections were acquired using a UniTom HR micro-CT

system (Tescan XRE nv, Ghent, Belgium) with voxel resolution of 3 µm for apple and 2.5 µm for pear. For the contrast-enhanced scan after the conventional scan, the tissue sample was carefully unwrapped and incubated in a 10% (w/v) cesium iodide solution for 1 (all pear cultivars and 'Jonagold') or 2 h ('Braeburn' and 'Kizuri') while agitating every 15 min.

After reconstruction, the corresponding 3D images were registered. From the conventional scan, the binary of the cell matrix and pore space were extracted using Otsu's thresholding. From the contrast-enhanced scan, the individual cell labels were extracted using a semi-automated cell segmentation workflow; the vasculature and stone cells were semi-manually segmented if present. Labeled images were used as ground truth for training the DL algorithm. Data was split into test, training and validation sets making sure datasets were from different fruit. Following the state-of-the art method for cell segmentation, the marker-based watershed algorithm was applied to the binary of the cell matrix as benchmark. As additional benchmark, an instance segmentation model trained on 2D data and enabling 3D prediction by averaging the 2D predictions in all orientations was included, to evaluate the cell segmentation accuracy.

Results

The panoptic segmentation model was able to segment following semantic labels: pore spaces, cell matrix, vascular bundles and clusters of stone cells (brachysclereids, only in pear tissue) and at the same time to predict intermediate representations of the instance labels, i.e. the cells, that allow cell reconstruction in a post-processing step. Thereto, it exploited the 3D extended version of the public domain Cellpose instance segmentation model, which in this study was adapted to a panoptic model after optimizing instance segmentation performance. The original instance segmentation model uses a 3D U-Net architecture to predict gradient map representations of cell instances. Following changes to this network architecture improved the instance segmentation accuracy: addition of long skip connections with direct summation, replacement of the standard building blocks with residual blocks whereby two consecutive residual blocks were implemented per layer, resulting in double the depth of the original 3D U-Net architecture, and retrieval of a style vector using global average pooling on the convolutional maps of the smallest dimension. The 3D model achieved Aggregated Jaccard Indices of 0.788 ± 0.061 and 0.889 ± 0.030 for pear and apple tissue, respectively, compared to 0.732 ± 0.075 and 0.861 ± 0.028 for the 2D model and 0.631 ± 0.134 and 0.715 ± 0.034 for the watershed-based benchmark. The 2D instance segmentation model was able to recognize vascular bundles and stone cell clusters and exclude them from the volume-of-interest. This demonstrated the potential to expand to panoptic segmentation combining semantic and instance segmentation tasks for the 3D model. However, prediction of the semantic labels was difficult as the dataset was highly

imbalanced. From the 810 training samples, 308 contain vasculature and/or stone cell clusters and if these labels were present, the occurrence based on the amount of voxels was much lower compared to the cell matrix and pore space labels. Focal loss was the most appropriate loss functions that learned the model to focus on the vascular bundles and stone cell clusters.

Conclusion

The 3D model succeeded in improving the cell segmentation accuracy over the 2D model and watershed-based benchmark. Cell segmentation remains more difficult for dense pear tissue compared to apple, but the 3D model showed greater improvement for pear tissue segmentation, reducing the difference between tissue types. The prediction of semantic labels is hindered by the large imbalance in the data. Therefore, further training wit data augmentation techniques have yet to confirm how much the focal loss can improve segmentation accuracy of vascular bundles and stone cells.

Graphic:

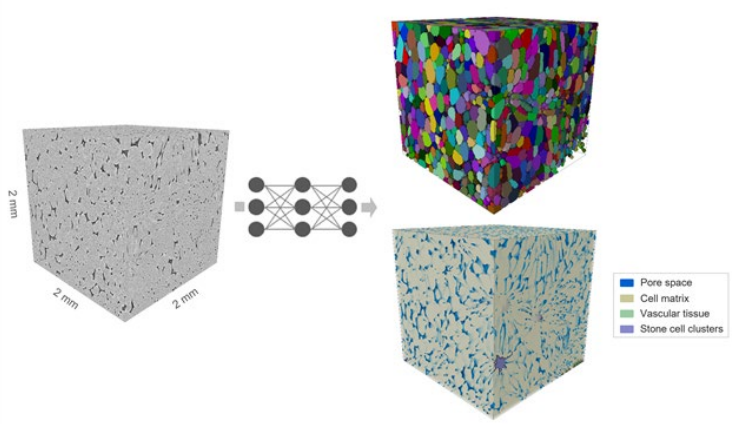

Keywords:

X-ray micro-CT, Image processing, AI

Reference:

Stringer C, Wang T, Michaelos M, Pachitariu M. Cellpose: a generalist algorithm for cellular segmentation. Nat Methods. 2021;18:100–6.
Eschweiler D, Smith RS, Stegmaier J. Robust 3D Cell Segmentation: Extending the View of Cellpose. In: IEEE International Conference on Image Processing. 2022. p. 191–5.
Van Doorselaer L, Verboven P, Nicolai B. Automatic 3D cell segmentation of fruit parenchyma tissue from X-ray micro CT images using deep learning. Plant Methods. 2024;20:1–19
Herremans E, Verboven P, Verlinden BE, Cantre D, Abera M, Wevers M, et al. Automatic analysis of the 3-D microstructure of fruit parenchyma tissue using X-ray micro-CT explains differences in aeration. BMC Plant Biol. 2015;15:1–15.